*applied sciences*

MDPI

*Article*

# Preparation and Performance of Core–Shell Structured B@$NiF_2$/AP Composite Micro-Units

**Jiaqi Cao [1,2,†], Yinhui Li [1,†], Changlin Zhu [3,†], Yunpeng Deng [1], Songyuchen Ma [1], Deqi Wang [1], Kunquan Duan [1] and Jie Liu [1,*]**

[1] National Special Superfine Powder Engineering Research Center of China, School of Chemistry and Chemical Engineering, Nanjing University of Science and Technology, Nanjing 210094, China; caojq@citic-hic.com.cn (J.C.); 15037810878@163.com (Y.L.); 18908483778@163.com (Y.D.); masongyuchen@163.com (S.M.); deqi_wang_njust@163.com (D.W.); kq1971306319@163.com (K.D.)
[2] CITIC Heavy Industries (Beijing) New Energy Material Technology Company, Beijing 102600, China
[3] School of Mechanical Engineering, Nanjing University of Science and Technology, Nanjing 210094, China; zhuchanglin@njust.edu.cn
* Correspondence: jie_liu_njust@126.com; Tel.: +86-025-84315042
† These authors contributed equally to this work.

**Abstract**

Boron (B) powder is a promising high-energy fuel but suffers from inefficient combustion due to its native boron oxide ($B_2O_3$) passivation layer. Surface coating is a crucial strategy to overcome this limitation. In this study, core–shell structured B@$NiF_2$/ammonium perchlorate (AP) composite micro-units with varying mass ratios were prepared using planetary ball milling to optimize energy release and combustion performance. The optimal formulation for the ternary composite was determined to be 0.5% $NiF_2$, 13.3% B, and 86.2% AP. Morphological characterization revealed that $NiF_2$ was uniformly coated on the B particles, forming a dense shell. Thermal analysis indicated that the $NiF_2$ interfacial layer, through its high-temperature decomposition ($NiF_2 \rightarrow Ni + 2F\cdot$), released highly reactive fluorine radicals (F·) that etched the $B_2O_3$ layer, generating volatile boron oxyfluoride and creating void structures. This led to a maximum heat release of 8912 J/g and a reaction mass gain of 74.58%, indicating more complete combustion. The material also exhibited a minimal ignition delay of 0.618 s and the lowest ignition energy (22.17 J). Overall, the B@$NiF_2$/AP composite provides a novel solution for applying boron fuel in solid propellants and pyrotechnic technologies.

**Keywords:** boron; surface coating; ignition performance; combustion rate; core–shell composite structure

check for updates

Received: 2 October 2025
Revised: 18 November 2025
Accepted: 24 November 2025
Published: 25 November 2025

**Citation:** Cao, J.; Li, Y.; Zhu, C.; Deng, Y.; Ma, S.; Wang, D.; Duan, K.; Liu, J. Preparation and Performance of Core–Shell Structured B@$NiF_2$/AP Composite Micro-Units. *Appl. Sci.* **2025**, *15*, 12495. https://doi.org/10.3390/app152312495

**Copyright:** © 2025 by the authors. Licensee MDPI, Basel, Switzerland. This article is an open access article distributed under the terms and conditions of the Creative Commons Attribution (CC BY) license (https://creativecommons.org/licenses/by/4.0/).

## 1. Introduction

Solid propellants serve as the power source for missiles, spacecraft launch vehicles, and rocket engines. With the advancement of aerospace technology, the demand for high-energy-density fuels has been continuously increasing. Boron (B) powder stands out as a prime candidate due to its exceptionally high volumetric and gravimetric calorific value (about 58.28 MJ/kg), which is nearly twice that of conventional aluminum fuels. However, the practical application of boron is severely hampered by a fundamental issue: a native, dense, and amorphous boron oxide ($B_2O_3$) layer that spontaneously forms on its surface. This passivation layer acts as a 'double-edged sword': it provides stability at room temperature but melts at moderate temperatures (~600–800 °C), forming a glassy encapsulating

layer that drastically delays ignition by hindering oxygen diffusion, ultimately leading to inefficient and incomplete combustion and preventing boron from realizing its full theoretical energy potential. Experiments have shown that boron powder with a diameter of 10 μm requires an environmental temperature exceeding 1900 K under standard atmospheric pressure to sustain combustion, which is significantly higher than the operating temperature of conventional propellants. The liquid oxide layer formed during combustion can also lead to particle agglomeration, reducing combustion efficiency and resulting in actual energy release only reaching 40–60% of the theoretical value.

According to previous literature, surface coating technologies can improve the ignition and combustion performance of metal fuels (Deng et al., 2018 [1]; Guo et al., 2012 [2]; He et al., 2020 [3]; Ma et al., 2020 [4]; Tang et al., 2020 [5]; Zhu et al., 2017 [6]). Metals (Weismiller et al., 2018) [7], metal anhydrides or oxides (Lee et al., 2019; Yuan et al., 2010) [8,9], rare earth metal catalysts (Cheng et al., 2020) [10], and fluorine-containing materials (Young et al., 2013) [11] have been used to coat boron particles. Relevant studies have shown (Matsumoto et al., 2003; Glotov et al., 2023) [12,13] that fluorides significantly improve the ignition and combustion of boron powder. They can react with the $B_2O_3$ oxide layer on the surface of boron particles, exposing the boron surface, thus accelerating the ignition of boron particles. The heat released during ignition further accelerates the reaction between the fluoride and the boron surface oxide. At the same time, the energy released from the formation of boron fluoride compounds by fluorine (F) and boron (B) per unit mass is much higher than the energy released from the formation of $B_2O_3$ by oxygen and boron powder, which greatly benefits overall energy enhancement.

By coating the surface with lithium fluoride or combining with magnesium-aluminum alloys, the ignition temperature can be reduced to below 1600 K. X-ray diffraction analysis shows that this treatment disrupts the continuity of the oxide layer. Synchrotron radiation diagnostic technology confirmed that the residence time of the modified boron powder in supersonic airflow is reduced to 2 ms, and the combustion efficiency is improved to over 85%. Test data released by Keerthi et al. (2020) [14] in 2022 shows that composite propellants containing 30% nano-boron achieve a specific impulse of 280 s, a 15% improvement over traditional formulations, marking a substantial advancement in the engineering application of boron-based fuels.

Beyond simple mixtures, engineered architectures like metastable intermolecular composites (MICs) have shown the profound impact of intimate reactant contact on combustion performance (He et al., 2018) [15], inspiring our design of an integrated core–shell structure.

The coating of boron particles with AP has been established as an effective strategy to enhance combustion performance. For instance, studies have demonstrated that AP-coated boron composites exhibit significantly improved combustion intensity and energy release output compared to their uncoated counterparts (Xie et al., 2014) [16]. Furthermore, research has highlighted that the mass ratio of the AP coating is a critical parameter, significantly influencing not only the combustion efficiency but also the practical processability of the resulting propellant mixtures. These prior works collectively underscore the importance of both intimate interfacial contact and optimized stoichiometry in unlocking the potential of boron fuels. Cheng et al. (2021) [17] prepared B/Mg, B/Al, B/Ni, B/Fe, and B/Mo composites using ball milling. Thermal analysis of Fe and Mo-doped boron powder indicated that boron powder has good reactivity and performance. Liu et al. (2024) [18] coated boron powder with halogenated compounds for high combustion efficiency and prepared four types of micro-nano B-Fe-$Bi_2O_3$@AP/PVDF composites. The highest combustion temperatures of these composites reached 1954–2011 °C, and the combustion efficiency was greatly improved in various atmospheres.

While the individual benefits of fluoride coatings and AP addition are well-established, a structure that intimately and synergistically integrates these two components at the micro-scale remains largely unexplored. The preceding literature clearly identifies two key bottlenecks: (1) the removal of the $B_2O_3$ layer, and (2) the efficient transfer of oxidizer to the fresh boron surface. Therefore, building upon these insights, this study proposes a novel core–shell structured B@$NiF_2$/AP composite micro-unit. We hypothesize that the $NiF_2$ interfacial layer will actively disrupt the passivation layer, while the nanoscale-intimate AP oxidizer shell will ensure a readily available oxygen supply, thereby synergistically overcoming both limitations simultaneously.

Therefore, to bridge this gap and address the unresolved challenge of creating an integrated fuel-fluorination-oxidizer system, Based on the high calorific value of boron and the strong oxidizing ability of AP, this study proposes a novel core–shell structure B@$NiF_2$/AP composite micro-unit design, aiming to break through the bottleneck of the oxide layer barrier in traditional boron-based fuels and the energy release efficiency of AP-based propellants. By introducing a nickel fluoride ($NiF_2$) interfacial layer, which utilizes its high-temperature fluorination reaction properties ($NiF_2 \rightarrow Ni + 2F\cdot$), the $B_2O_3$ passivation layer is directionally destroyed and fluorine radicals are released. This simultaneously enhances the ignition and accelerates the combustion of boron particles. Meanwhile, AP, as the oxidizer shell, is coated, and through the nanoscale intimate contact between the oxidizer and fuel inside the micro-unit, the oxygen transfer path is shortened, reducing the diffusion combustion lag effect. This multi-scale synergistic strategy greatly improves the combustion efficiency of boron. This study constructs the core–shell micro-unit structure using a planetary ball milling process, combined with thermodynamic testing and ignition combustion analysis, revealing the coupling mechanism of fluorination interfacial reaction kinetics and energy release, providing theoretical support and material paradigms for the design of the next generation of high-energy, low-signature solid propellants.

## 2. Experimental Section

### 2.1. Experimental Materials

Amorphous boron powder (amorphous B powder, D50 = 2.731 μm, where D50 represents the median particle diameter) was provided by the Hubei Aerospace Chemical Technology Research Institute (Xiangyang City, China). AP ($NH_4ClO_4$, D50 = 188.351 μm) was purchased from Dalian Northern Potassium Perchlorate Factory. Nickel fluoride ($NiF_2$, D50 = 3.462 μm) was purchased from Nanjing Chemical Reagent Co., Ltd. (Nanjing, China).

### 2.2. Preparation Process of B@$NiF_2$/AP Composite Micro-Units

The samples were prepared using a planetary ball milling method. First, 1.0000 g of amorphous boron powder was accurately weighed using an electronic balance with a precision of 0.0001 g, and the corresponding amounts of $NiF_2$ (2%, 4%, 8%, 12%, and 16% by weight) were precisely weighed. The weighed amorphous boron powder and $NiF_2$ were placed in a 100 mL ball milling jar and subjected to ball milling using a QM-2SP4 planetary ball mill (QC Group Limited, Newry, Ireland). To control experimental variables, all samples underwent the same ball milling procedure, with a set speed of 300 rpm, ensuring the independent investigation of the effect of different $NiF_2$ incorporation levels on the performance of boron powder. The various ball milling parameters are as follows: zirconia beads with a diameter of 0.8 mm were used, the ball-to-powder ratio was set at 20:1, and the ball milling duration was 3 h. After milling, the samples were sieved through a 90-mesh screen and divided into portions for subsequent performance characterization.

Subsequently, the B@$NiF_2$ core–shell structure with a 4% $NiF_2$ content was selected as the fuel component for preparing the ternary composite. To determine the optimal

proportion of oxidizer (AP) to fuel (B@$NiF_2$), we applied the oxygen balance theory. The objective of oxygen balance is to provide just enough oxygen from the oxidizer to completely convert all fuel elements (B, C, H, etc.) to their most stable oxidation products (e.g., $B_2O_3$, $CO_2$, $H_2O$). For the B@$NiF_2$/AP system, the calculation primarily considers the complete oxidation of boron and the decomposition products of AP. Based on this principle, a series of AP to B@$NiF_2$ ratios (5:1, 6:1, 6.6:1, 8:1, and 9:1) were designed and tested. The stoichiometric ratio of 6.5:1 (equivalent to 0.5% $NiF_2$, 13.3% B, and 86.2% AP in the final formulation) was identified as the oxygen-balanced point for this specific system and was therefore investigated in depth. The B@$NiF_2$ core–shell structure and AP were accurately weighed.

### 2.3. Sample Characterization

The morphology of the composite micro-units was observed and recorded using a Hitachi Regulus 8100 X-raymicroscope (SEM) produced by Hitachi (Tokyo, Japan). During the test, a small amount of powder sample was uniformly dispersed on conductive tape, and the sample was gold-coated for 45 s under a current of 10 mA using an Oxford Ultim Max 65 sputter coater (Oxford Instruments, Oxford, UK) to enhance its conductivity. The test conditions were set as follows: acceleration voltage of 3 kV, and for energy spectrum mapping, the acceleration voltage was set to 20 kV. The SE2 secondary electron detector was used to obtain high-resolution images at different magnifications.

The surface structure, elemental valence states, and content of the composite micro-units were semi-quantitatively analyzed using a Thermo Scientific K-Alpha X-ray photoelectron spectrometer (XPS) (Thermo Scientific, Waltham, MA, USA). The tests were conducted using Al K$\alpha$ radiation (hv = 1486.6 eV), with a working voltage of 12 kV and filament current of 6 mA.

To investigate the thermal behavior of the samples, a TA Instruments SDT 650 thermogravimetric-differential scanning calorimeter (TG-DSC) (TA Instruments, New Castle, DE, USA) was used to characterize the thermal and kinetic properties of the samples. Approximately 1.5 mg of the sample was tested in an air atmosphere at a gas flow rate of 50 mL/min. The sample was placed in an alumina crucible and heated at a rate of 20 °C/min from 50 °C to 1200 °C. Prior to testing, the thermal analyzer was mass-calibrated using standard mass weights (with a sensitivity of 0.1 μg for the thermal balance) and calibrated for heat flow using sapphire. The raw data were processed and analyzed using Universal Analysis 2000 software.

To further investigate the heat release properties of the samples, an IKA C3000 isoperibol calorimeter, produced by IKA Works GmbH & Co. (Staufen im Breisgau, Germany), was used to measure the combustion heat of the samples. Based on the measurable energy range of the calorimeter, approximately 300 mg of the sample was tested in a high-concentration oxygen atmosphere. The sample was ignited using a platinum wire and ignition cotton wick, and combustion occurred within a sealed bomb calorimeter. The cotton wick had a heat value of 50 J/g.

The ignition and combustion performance of the samples was evaluated using a custom-built combustion testing system (schematic shown in Figure 1). The tests were conducted in a sealed combustion chamber with an internal volume of approximately 0.5 L, under ambient atmospheric conditions (in air) at room temperature (~25 °C) [19,20]. First, 30 mg of the sample was placed on the ignition platform, and a 0.25 mm nichrome wire was passed through the sample and wound onto the ignition electrode. The sample was rapidly heated and ignited with a constant pressure power supply (15 V). During this process, a TELEDYNE WAVESURGER3054 oscilloscope (Teledyne LeCroy, Chestnut Ridge, NY, USA) received optical signals from a light sensor (Thorlabs DETO2AFC, Newton, NJ, USA)

and electrical signals transmitted from the ignition electrode. The current, pressure, and light signals generated by the sample combustion were displayed on the oscilloscope. The minimum energy required for ignition was calculated using the ignition energy formula, as shown in Equation (1). The ignition delay time, denoted as $t$ (s), was defined as the time required from the generation of current to the sudden increase in the optical signal. The DC voltage applied to the circuit was $U$ (V), and the current in the circuit was $I$ (A). Typical voltage, current, light signals, and ignition delay time for open ignition combustion tests were recorded. Each sample was tested 3–5 times, and the average value of three data sets with a standard deviation between 0 and 0.5 was retained.

$$E = \int_0^t UIdt \quad (1)$$

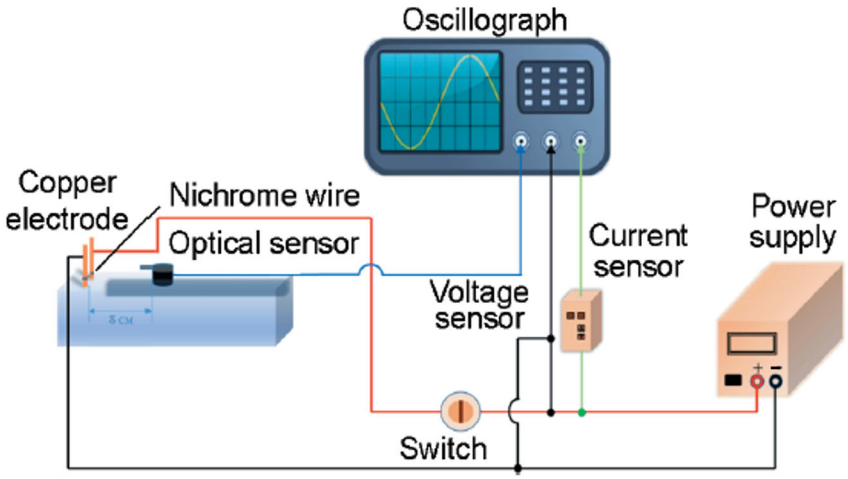



**Figure 1.** Schematic diagram of the custom-built combustion testing system (Liu et al., 2024) [21].

At the same time, a high-speed camera system from PHOTRON, Tokyo, Japan, the Photron UX100, along with data acquisition and analysis software, was used to capture the flame characteristics and ignition performance of the sample. The recording speed was set to 2000 fps.

## 3. Results and Discussion

### *3.1. Morphology and Structure*

The morphology of the B@$NiF_2$ composite materials at different ratios and the raw B material was observed using the planetary ball milling technique. The test results are shown in Figure 2.

Figure 2f shows the SEM image of the raw B powder. Figure 2a indicates that when the $NiF_2$ content is insufficient, the product exhibits significant inhomogeneity: apparent exposed areas and gaps are observed between the particulate phases, suggesting that the coating process is less effective at this low ratio. This structural defect leads to the scattering of a large number of unbound particles on the surface.

In contrast, Figure 2b–d show a more homogeneous morphology with significantly fewer scattered particles. A more continuous and adhered layer is observed on the particulate surfaces, which is consistent with the formation of a composite structure. The particle sizes appear larger than the raw boron, indicating the formation of composite agglomerates during ball milling. This structural feature is favorable for the formation of a dense protective layer. Comparing the different samples, the areas of the fitted peaks for each bond type were compared. For the composite micro-unit at 4% $NiF_2$, the $B_2O_3$ content on the surface was lower, at 8.5%, and the characteristic peak area for elemental B-B reached the highest level at 60.0%. This surface composition, characterized by the highest

relative content of elemental boron, is considered favorable for subsequent energy release. The uniform mixture observed in SEM images (Figure 2b–d) is attributed to the efficient mechanical blending achieved during the ball milling process.

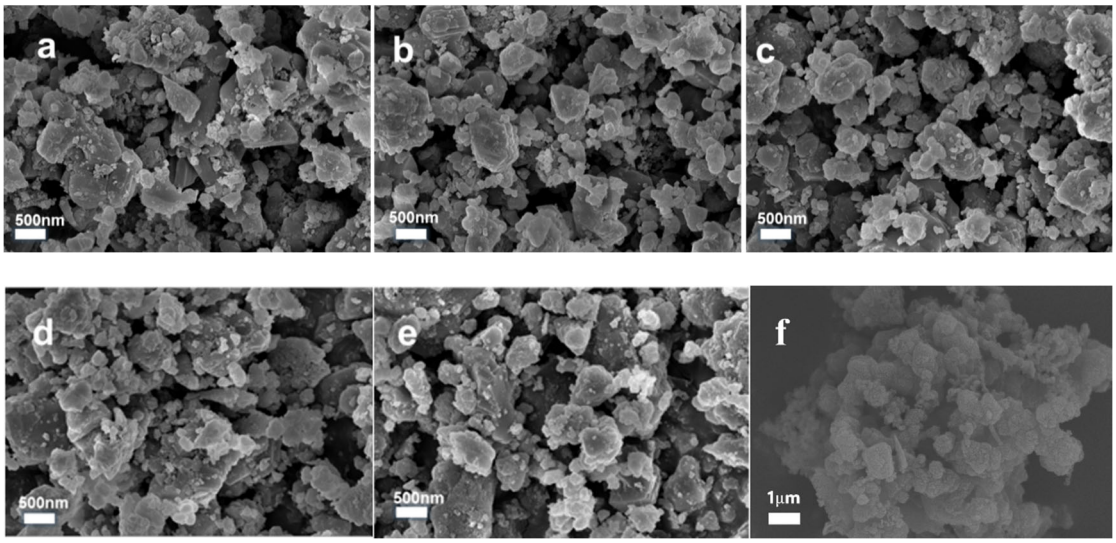



**Figure 2.** Comparison of SEM morphology of B@$NiF_2$ composites with different $NiF_2$/B ratios: (**a**) B@$NiF_2$-2%; (**b**) B@$NiF_2$-4%; (**c**) B@$NiF_2$-8%; (**d**) B@$NiF_2$-12%; (**e**) B@$NiF_2$-16%; (**f**) Raw B material.

At the highest $NiF_2$ content (16%, Figure 2e), the particulate surfaces are fully covered, but with a substantial amount of additional granular material. This suggests the formation of a thick coating layer, resulting in composite agglomerates with the largest overall size among the samples. This prevents the micro-nano materials' small size and rapid energy release from being fully utilized. Additionally, the excessive shell thickness negatively impacts the stability of the subsequent B@$NiF_2$/AP composite micro-unit structure formed with the added oxidizer AP.

From Figure 3a–g, it can be seen that as the $NiF_2$ content increases, the B-B bond content in the sample shows a trend of first increasing and then decreasing. Additionally, the $B_2O_3$ content also shows significant changes at different $NiF_2$ incorporation levels, with noticeable fluctuations in the impurity Bx-O bond content. This indicates that the incorporation of $NiF_2$ affects the surface oxidation of the boron powder.

With $NiF_2$ contents of 2%, 4%, 8%, 12%, and 16%, the Bx-O content gradually increased from 31.9% at 2% incorporation to a maximum of 59.7% at 12%, indicating that excessive $NiF_2$ incorporation accelerates the hybridization reaction of boron powder. At different incorporation levels, the $B_2O_3$ content was relatively low at 2% incorporation (8.4%), and as the incorporation amount increased, the $B_2O_3$ content at 4% $NiF_2$ incorporation remained low at 8.5%, before showing an increasing trend. The variation in $B_2O_3$ content with different $NiF_2$ incorporation levels indicates that the incorporation of $NiF_2$ alters the surface chemistry of the boron powder. The B-B bond content gradually decreased with increasing $NiF_2$, indicating that $NiF_2$ promotes the oxidation of boron powder to some extent.

Comparing the different samples, the areas of the fitted peaks for each bond type were compared. For the composite micro-unit at 4% $NiF_2$, the $B_2O_3$ content on the surface was lower, at 8.5%, and the characteristic peak area for elemental B-B reached the highest level at 60.0%. This surface composition, characterized by a high content of elemental boron and a relatively low content of oxide, is considered favorable for subsequent energy release, which is consistent with the superior thermal performance (e.g., highest heat release of 8912 J/g) observed for the BN-2 sample in Section 3.2. The uniform mixture

achieved during ball milling, as seen in the SEM images, likely contributed to this distinct surface chemistry.

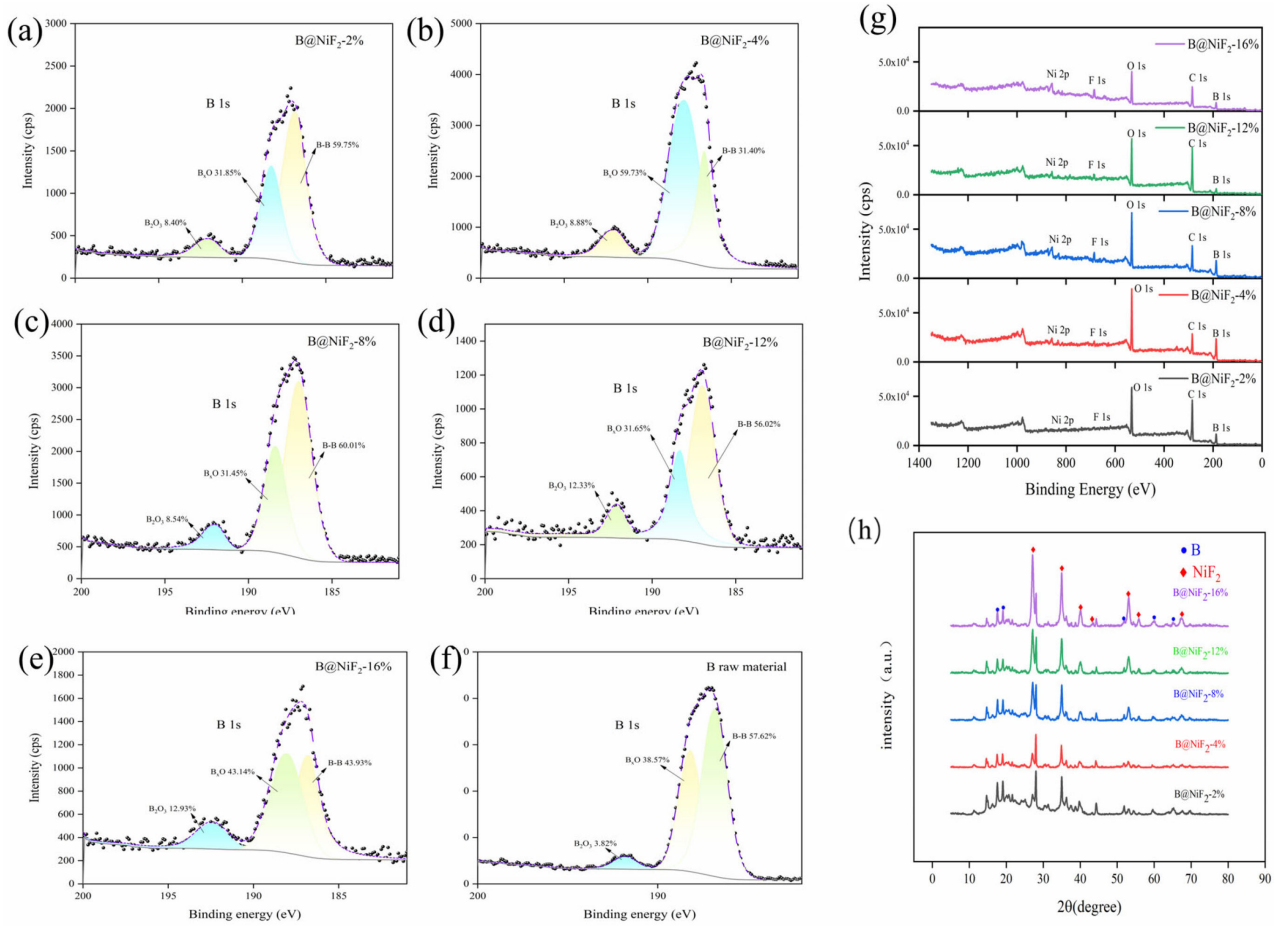



**Figure 3.** Sample Phase Characterization Plots: (**a**–**f**) High-resolution B1s spectra of B@$NiF_2$ at different $NiF_2$ formulation ratios; (**g**) XPS full spectra of B@$NiF_2$ at different $NiF_2$ formulation ratios; (**h**) XRD spectra of the scanned B@$NiF_2$ sample.

Figure 3h shows that the different $NiF_2$ formulation ratios have little effect on the peak shape, but they significantly influence the peak area and peak height. As the $NiF_2$ ratio increases, the corresponding peak area and peak height for $NiF_2$ also increase, confirming its increasing presence in the composite. The peak shapes for all the samples are consistent. The XRD patterns confirm the coexistence of crystalline boron and nickel fluoride ($NiF_2$) phases in all ball-milled samples, with no other crystalline impurities detected.

The morphological observations from SEM, combined with the surface chemical analysis from XPS and the phase identification from XRD, collectively provide compelling, multi-faceted evidence for the formation of a core–shell-type structure in the B@$NiF_2$ composites. This structural configuration is posited as the foundation for the significantly enhanced combustion performance detailed in the following sections.

### *3.2. Thermal Behavior Analysis of B@$NiF_2$*

The DSC curves for samples with different $NiF_2$ contents are presented in Figure 4a. All samples exhibit a primary exothermic peak, although the peak shapes and temperatures vary. The peak temperatures (Tp) for the major exotherm are identified at 750.2 °C for BN-1, 749.5 °C for BN-2, 750.2 °C for BN-3, 671.1 °C for BN-4, and 653.7 °C for BN-5. However, with increasing $NiF_2$ content, the exothermic peak shifts to an earlier temperature. From the TG curve, it can be observed that the sample weight decreases with increasing temperature

before 560 °C. According to the literature [22–24], the continuous weight loss between 300 °C and 560 °C is consistent with the reported decomposition behavior of $NiF_2$. The subsequent weight gain after 560 °C, accompanied by a sharp exotherm, suggests the occurrence of the oxidation reaction between boron and oxygen, leading to the formation of $B_2O_3$.

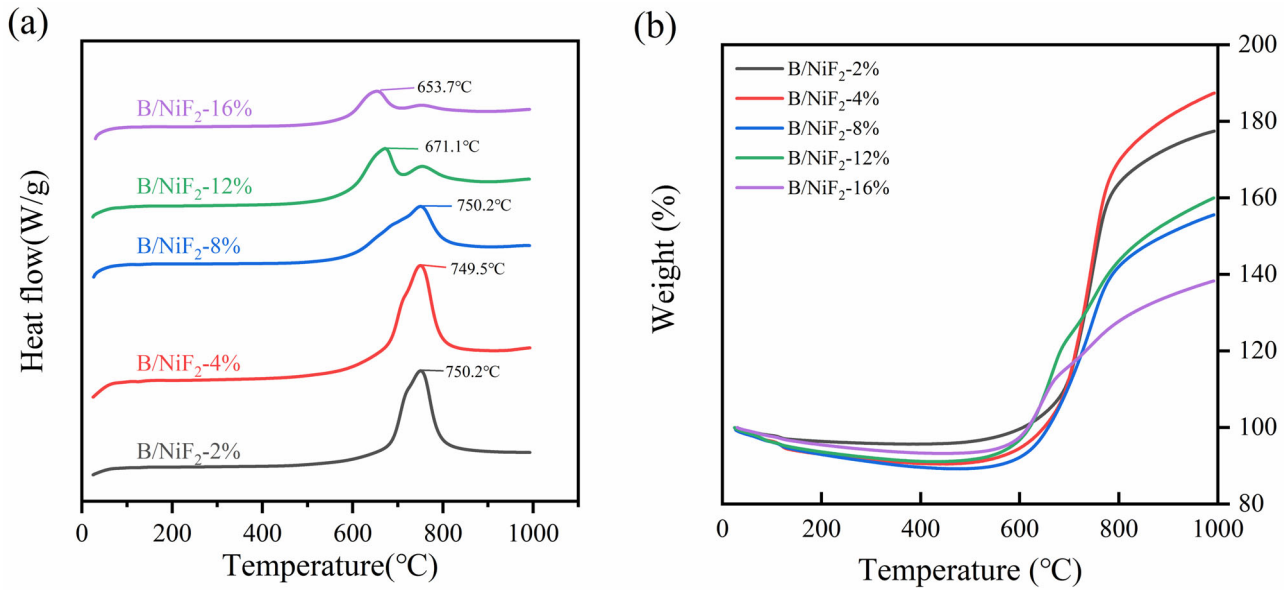



**Figure 4.** (**a**) DSC curves of B@$NiF_2$ with different stoichiometric ratios; (**b**) TG curves of B@$NiF_2$ with different stoichiometric ratios.

As shown in Table 1, the exothermic peak temperatures of the samples under different $NiF_2$incorporationlevels are generally consistent. However, when the $NiF_2$ incorporationlevel is 4%, the exothermic energy of the sample reaches the maximum value of 8912 J/g, which is more than 7% higher than that of the samples with other incorporation ratios. At the same time, the oxidation weight gain rate of this sample also reaches the highest value of 74.6%, which is more than 9.0% higher than that of the other samples. The systematic downward shift in the major exothermic peak temperature with increasing $NiF_2$ content, as observed in Figure 4a and Table 1, can be attributed to the reactive role of $NiF_2$ in disrupting the passivating $B_2O_3$ layer. The initial mass loss in the TG curves (300–560 °C) is associated with the decomposition of $NiF_2$, which liberates highly reactive fluorine species. These fluorine species then chemically attack the $B_2O_3$ layer, as described by the reaction proposed in Section 3.5 ($NiF_2 + 2B_2O_3(l) \rightarrow Ni(BO_2)_2 + 2BOF(g)$). This reaction consumes the solid oxide barrier, generating volatile products and creating pathways for oxygen diffusion. Consequently, a higher loading of $NiF_2$ leads to a more extensive and earlier removal of the $B_2O_3$ layer during the heating process, thereby facilitating the onset of the main boron-oxygen oxidation reaction at a progressively lower temperature. This mechanism is consistent with the known efficacy of fluorides in enhancing boron ignition (Glotov et al., 2023) [13].

This result indicates that the introduction of $NiF_2$ significantly enhances the heat release of the boron powder and increases its degree of reaction. Among the five groups of samples, the 4% $NiF_2$incorporationlevel optimizes both the heat release performance and the degree of reaction of the sample.

**Table 1.** Thermal Analysis Data of B@$NiF_2$ with Different Stoichiometric Ratios.

| Sample | $T_p$/°C | $Q$/J $g^{-1}$ | $\Delta m$/% |
|---|---|---|---|
| BN-1 | 750.2 | 8332 | 68.40 |
| BN-2 | 749.5 | 8912 | 74.58 |
| BN-3 | 750.2 | 5552 | 52.31 |
| BN-4 | 671.1 | 5587 | 52.81 |
| BN-5 | 753.7 | 1840 | 34.42 |

Note: In this table, the sample nomenclature 'BN-1' to 'BN-5' corresponds to B@$NiF_2$ composites with $NiF_2$ contents of 2%, 4%, 8%, 12%, and 16%, respectively. Tp refers to the temperature at the exothermic peak for each sample, and $\Delta m$ represents the mass change percentage of each sample at 1000 °C.

The data from the bomb calorimeter in Table 2 provides further insight into the energy release. The BN-1 sample (2% $NiF_2$) exhibits the highest combustion heat (14,875 J/g), which is consistent with its highest content of elemental boron fuel. However, it is crucial to consider this value in conjunction with the reaction efficiency revealed by TG-DSC (Table 1). The BN-2 sample (4% $NiF_2$), although it has a slightly lower combustion heat (14,657 J/g), demonstrates the most complete oxidation reaction (highest mass gain of 74.58%) and the largest exothermic enthalpy (8912 J/g) as shown in Table 1. This indicates that the 4% $NiF_2$ formulation achieves an optimal balance, effectively enhancing the combustion efficiency of boron without a substantial sacrifice in the overall energy output.

**Table 2.** Bomb Calorimeter Data of B@$NiF_2$ with Different Stoichiometric Ratios.

| Sample | BN-1 | BN-2 | BN-3 | BN-4 | BN-5 |
|---|---|---|---|---|---|
| **Heat Release (J/g)** | 14,875 | 14,657 | 14,105 | 13,799 | 13,455 |
| **Number of Replicates (*n*)** | 3 | 3 | 3 | 3 | 3 |

Notes: Values for ignition delay time and energy are presented as mean ± SD from n independent tests.

Based on the performance results of the BN samples, the most suitable B@$NiF_2$ sample, BN-2, was selected. After determining the appropriate ratio, the oxidizer AP was added according to the steps mentioned above to prepare the ternary B@$NiF_2$/AP composite micro-unit structure (BNA sample). The thermal properties and ignition combustion performance of the BNA sample were then characterized and analyzed.

The performance of the optimal B@$NiF_2$ composite (BN-2) compares favorably with other modified boron materials reported in recent literature. For instance, its heat release of 8912 J/g (from DSC) and 14,657 J/g (from bomb calorimetry) are competitive with or exceed values reported for boron-based composites such as B/Mg and B/Al (Cheng et al., 2021) [17], and those coated with fluoropolymers (Keerthi et al., 2020) [14]. This highlights the effectiveness of the $NiF_2$ coating and the planetary ball milling process in creating a high-energy material with enhanced combustion characteristics.

### *3.3. Thermal Behavior Analysis of B@$NiF_2$/AP*

To investigate the effect of different AP incorporation levels on the thermal performance of B@$NiF_2$, differential DSC-TG was used for thermal characterization. The experimental results are shown in Figure 5. The DSC curves under different AP incorporation levels exhibit similar characteristics. When heated in an air atmosphere, all the samples show a small endothermic peak around 250 °C, accompanied by a slight weight loss, which is attributed to the endothermic decomposition of AP. Subsequently, around 380 °C, a significant exothermic reaction occurs, accompanied by a sharp weight loss, indicating that the sample undergoes a vigorous exothermic reaction and generates a large amount of gas. Finally, around 770 °C, all samples exhibit a pronounced exothermic peak along with a

significant weight gain. This phenomenon corresponds to the oxidation reaction of the boron powder and the associated exothermic process.

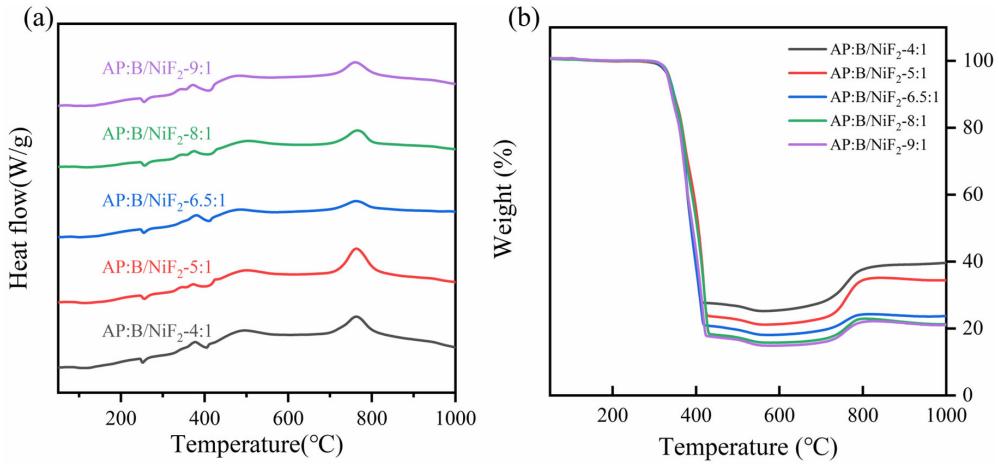



**Figure 5.** (**a**) DSC curves of different AP and B@$NiF_2$ mixing ratios; (**b**) TG curves of different AP and B@$NiF_2$ mixing ratios.

From the data in Table 3 and Figure 5a,b, it can be seen that samples with different AP incorporation levels exhibit similar reaction temperatures. When the stoichiometric ratio of AP to B@$NiF_2$ is 6.5:1, the sample's heat release reaches the maximum value of 635 J/g, which is more than 1.9% higher than that of the other samples. The weight change, as an indicator of the degree of reaction, shows minimal differences between the five groups of samples. Considering the data from the heat release, reaction temperature, and weight change, the sample with a stoichiometric ratio of 6.5:1 shows the best thermal performance. The experimental results indicate that the addition of AP as an oxidizer significantly improved the thermal performance of the B@$NiF_2$ mixture, with the 6.5:1 stoichiometric ratio being the optimal incorporation ratio.

**Table 3.** Thermal Analysis Data for Different AP and B@$NiF_2$ Mixing Ratios.

| AP:B@$NiF_2$ | $T_p$/°C | $Q$/J·g$^{-1}$ | $\Delta m$/% |
|---|---|---|---|
| 4:1 | 774.5 | 578 | 62.73 |
| 5:1 | 778.3 | 623 | 67.47 |
| 6.5:1 | 777.8 | 635 | 77.32 |
| 8:1 | 781.2 | 609 | 79.11 |
| 9:1 | 781.8 | 583 | 79.03 |

To further investigate the thermal performance of the AP-doped samples, the combustion heat release of the samples was measured using a bomb calorimeter.

From Table 4, it can be seen that as the AP incorporation level increases, the heat release of the samples decreases. When the stoichiometric ratio of AP to B@$NiF_2$ is 6.5:1, the heat release decreases significantly.

The experimental results reveal the distinct roles of composition in energy content and combustion efficiency. The bomb calorimeter data (Table 4) shows that formulations richer in the B@$NiF_2$ fuel (4:1 and 5:1 ratios) yield higher total energy release, which is attributed to their greater mass fraction of high-enthalpy boron. However, a comprehensive evaluation that prioritizes efficient and rapid energy release—key for propellant applications—must include ignition and combustion kinetics. In this regard, the 6.5:1 ratio, formulated based on oxygen balance, demonstrates an outstanding balance. While its absolute energy is lower, it exhibits a strong DSC exotherm (635 J/g, Table 3) and, most critically, it delivers

the best ignition and combustion performance, as evidenced by the shortest ignition delay, lowest ignition energy (Section 3.4, Table 5, Figure 6f), and a more complete combustion profile (Figure 7c). This indicates that the 6.5:1 ratio optimally utilizes the AP oxidizer to enhance the combustion efficiency of the B@$NiF_2$ fuel, achieving superior synergistic performance. Therefore, the 6.5:1 ratio was selected for the ternary composite as it best fulfills the design goal of achieving rapid and vigorous combustion.

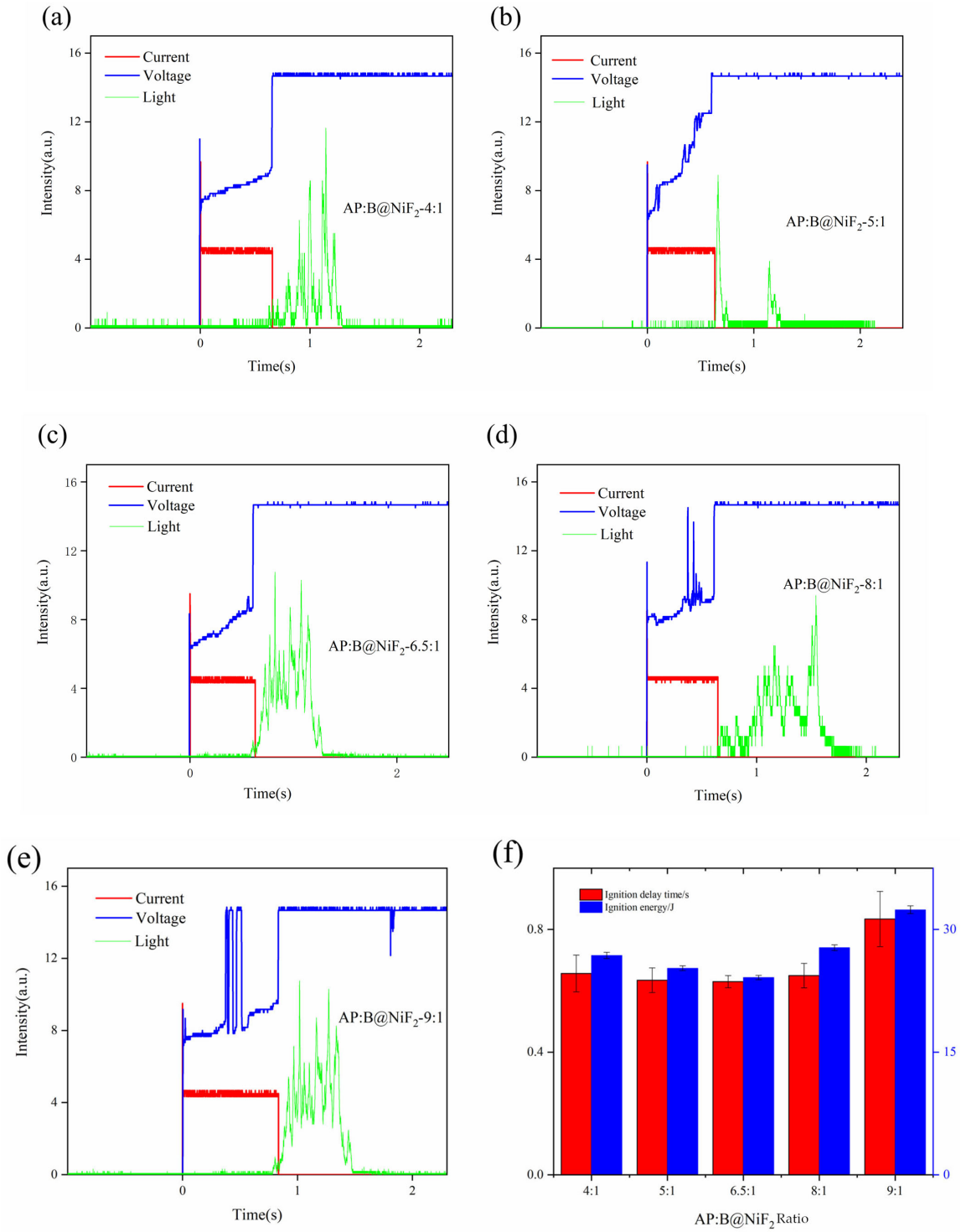



**Figure 6.** (**a**–**e**) Schematic of ignition signals for different AP and B@$NiF_2$ ratios in an open environment; (**f**) Ignition delay time and ignition energy graph.

**Table 4.** Bomb Calorimeter Data of B@$NiF_2$ with Different AP incorporation Ratios.

| AP:B@$NiF_2$ | 4:1 | 5:1 | 6.5:1 | 8:1 | 9:1 |
|---|---|---|---|---|---|
| Heat Release (J/g) | 9442 | 9273 | 7731 | 7780 | 7297 |
| **Number of Replicates (*n*)** | 3 | 3 | 3 | 3 | 3 |

Notes: Values for ignition delay time and energy are presented as mean ± SD from n independent tests.

**Table 5.** Ignition Performance Data for Samples with Different AP/B@$NiF_2$ Ratios.

| Sample | Ignition Delay Time (s) | Standard Deviation (SD) | Ignition Energy (J) | Standard Deviation (SD) |
|---|---|---|---|---|
| 4:1 | 0.673 | 0.11 | 33.81 | 0.47 |
| 5:1 | 0.652 | 0.09 | 28.64 | 0.35 |
| 6.5:1 | 0.618 | 0.03 | 22.17 | 0.23 |
| 8:1 | 0.661 | 0.08 | 26.42 | 0.39 |
| 9:1 | 0.818 | 0.17 | 27.53 | 0.51 |

Notes: Values for ignition delay time and energy are presented as mean ± SD from n independent tests.

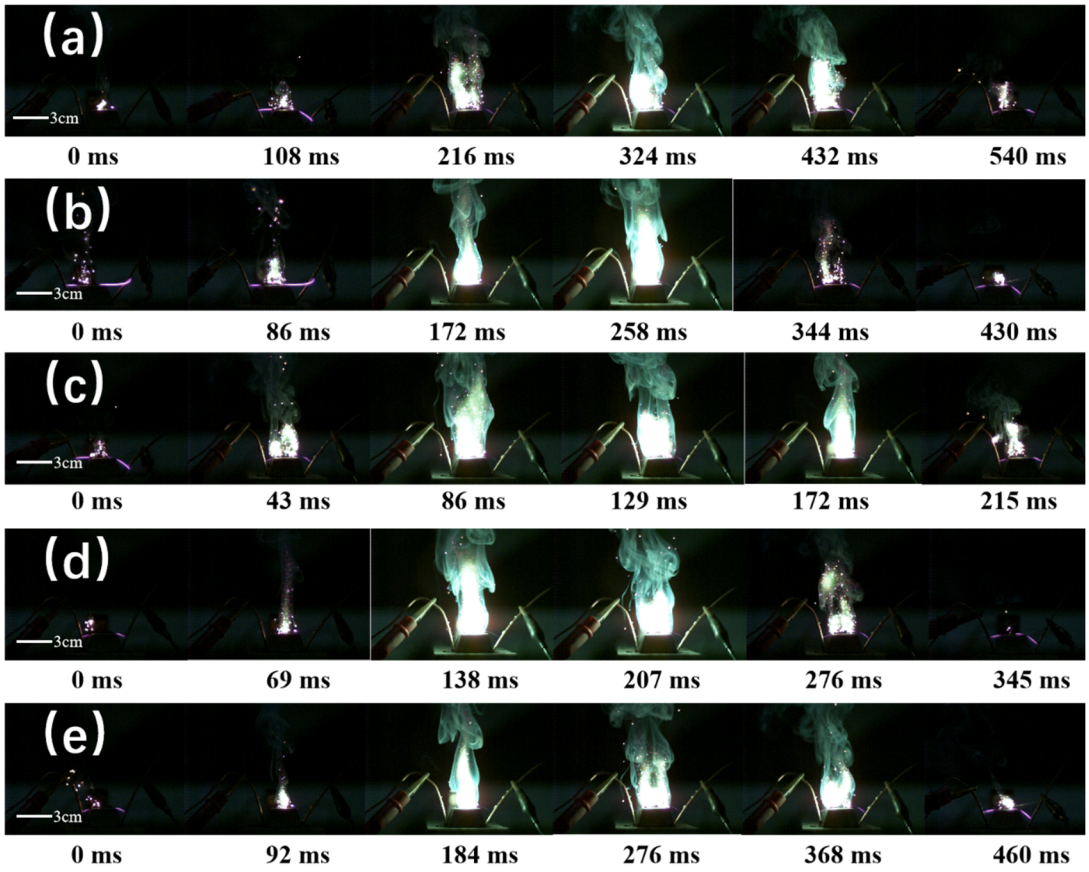



**Figure 7.** High-speed photographic images of combustion at atmospheric pressure for different AP:B@$NiF_2$ ratios. (**a**) 4:1, (**b**) 5:1, (**c**) 6.5:1, (**d**) 8:1, (**e**) 9:1.

### *3.4. Effect of AP Content on the Ignition and Combustion Performance of B/$NiF_2$/ AP Modified Composite Micro-Units*

From Figure 6a–f and combined with the data in Table 5, it can be observed that the incorporation of AP at different stoichiometric ratios has a significant impact on the ignition performance of B@$NiF_2$. Among the samples, the 6.5:1 formulation exhibits the shortest mean ignition delay (0.618 s). This value is not only lower than that of other ratios but is also associated with the smallest standard deviation (0.03 s, see Table 5), indicating superior and highly consistent ignition performance. The combination of a low mean delay and minimal

variance underscores the effectiveness of this oxygen-balanced formulation in achieving rapid and reliable ignition. Although the samples with 8:1 and 9:1 incorporation ratios also exhibit good performance in terms of ignition light intensity signals, the 6.5:1 incorporation ratio samples not only have excellent ignition light intensity and lower ignition delay, but their combustion time is also significantly prolonged. This suggests that the combustion process of the sample at this ratio is more uniform and complete.

As shown in Figure 6f and Table 5, the ignition energy of the AP and B@$NiF_2$ composite varies with the Ap incorporation content, first decreasing and then increasing. At the 6.5:1 incorporation ratio, the ignition energy reaches its lowest value, indicating that the incorporation ratio based on oxygen balance calculations has a promoting effect on the combustion of the modified boron powder.

From Figure 7, the combustion behavior of the B@$NiF_2$@AP core–shell structure at different AP:B@$NiF_2$ ratios can be observed. Figure 7b,c show relatively clear and complete flame profiles at 121 ms and 310 ms, with a flame height of approximately 30 mm. However, in Figure 7c, the green edge around the flame is significantly less than in Figure 7b, indicating a relatively lower generation of the incomplete combustion product $BO_2$. Additionally, Figure 7c shows a more complete and faster ignition and combustion process, with the flame intensity reaching its peak at 129 ms. This phenomenon suggests that at this ratio, the combustion process has a larger combustion area, stronger flame intensity, and shorter ignition and combustion times. Moreover, the reduced generation of incomplete combustion products, such as $BO_2$, leads to more complete combustion, resulting in superior ignition and combustion performance.

### *3.5. Preliminary Exploration of the Reaction Mechanism of B/Metal Fluoride*

Based on the TG-DSC results (significant mass loss and exothermic peaks) and supported by previous studies on metal fluorides [25–29], a potential reaction mechanism for the B/$NiF_2$ system is proposed. It is hypothesized that during heating, $NiF_2$ undergoes thermal decomposition, releasing highly reactive fluorine radicals (F·). These radicals then likely react with the native $B_2O_3$ layer on the boron surface, generating volatile boron oxyfluoride (BOF) gas, as represented in Reaction (2). This process is believed to disrupt the passivating oxide layer, exposing fresh boron to oxidizer and facilitating ignition and combustion. The energy released from the fluorination reactions, which is higher per unit mass than oxidation, contributes to the overall energy output. While the collective evidence from morphology, surface chemistry, and performance strongly supports the proposed core–shell model and reaction mechanism, direct visualization of the core–shell interface via cross-sectional transmission electron microscopy (TEM) in future work would provide the ultimate confirmation. We note that this proposed pathway is inferred from thermal analysis and the literature, and direct experimental validation, such as quenching and product analysis, would be valuable to confirm it in future work.

$$NiF_2 + 2B_2O_3(l) \rightarrow Ni(BO_2)_2 + 2BOF(g) \quad (2)$$

## 4. Conclusions

In this study, a novel core–shell structured B@$NiF_2$/AP composite micro-unit was designed and prepared. A combination of SEM, XPS, and XRD characterization strongly suggests the successful formation of this architecture. Based on the optimized binary B@$NiF_2$ structure, the optimal mass ratio of AP to B@$NiF_2$ was determined to be 6.5:1, corresponding to an overall formulation of 0.5% $NiF_2$, 13.3% B, and 86.2% AP. During the ignition and combustion process, the $NiF_2$ interfacial layer, through its high-temperature fluorination reaction ($NiF_2 \rightarrow Ni + 2F\cdot$), releases highly electronegative fluorine radicals that

react to form boron oxyfluoride gas and create void structures, leading to full exposure of the boron surface. AP further enhances the etching and activation effect, thereby shortening the ignition phase and significantly improving the ignition and combustion performance of boron powder. The core–shell structured B@$NiF_2$/AP composite micro-unit provides a novel solution for the application of boron fuel in solid propellants and pyrotechnics and establishes the optimal mass ratio for this ternary composite system. Furthermore, while direct measurement was beyond the scope of this study, the morphological evolution observed via SEM suggests that the ball-milling process and compositional changes significantly alter the specific surface area of the composites, which is expected to be a contributing factor to the enhanced ignition and combustion kinetics. A quantitative investigation of the surface area and its correlation with performance represents an important direction for future research.

**Author Contributions:** Conceptualization, J.L. and Y.L.; Methodology, J.C., Y.L. and C.Z.; Validation, Y.D. and S.M.; Formal Analysis, D.W. and K.D.; Investigation, J.C., Y.L. and C.Z.; Resources, J.L.; Data Curation, Y.D. and S.M.; Writing—Original Draft Preparation, Y.L.; Writing—Review and Editing, J.C. and J.L.; Visualization, C.Z.; Supervision, J.L.; Project Administration, J.L.; Funding Acquisition, J.L. All authors have read and agreed to the published version of the manuscript.

**Funding:** This paper received funding from the Special Fund for Basic Research Business of Central Universities, No. 30924010908.

**Institutional Review Board Statement:** Not applicable.

**Informed Consent Statement:** Not applicable.

**Data Availability Statement:** The original contributions presented in this study are included in the article. Further inquiries can be directed to the corresponding author.

**Conflicts of Interest:** Author Jiaqi Cao was employed by the company CITIC Heavy Industries (Beijing) New Energy Material Technology Company. The remaining authors declare that the research was conducted in the absence of any commercial or financial relationships that could be construed as a potential conflict of interest.

## References

1. Deng, S.; Jiang, Y.; Huang, S.; Shi, X.; Zhao, J.; Zheng, X. Tuning the morphological, ignition and combustion properties of micron-Al/CuO thermites through different synthesis approaches. *Combust. Flame* **2018**, *195*, 303–310. [CrossRef]
2. Guo, R.; Hu, Y.; Shen, R.; Ye, Y.; Wu, L. A micro initiator realized by integrating KNO3@CNTs nanoenergetic materials with a Cu microbridge. *Chem. Eng. J.* **2012**, *211–212*, 31–36. [CrossRef]
3. He, W.; Li, Z.-H.; Chen, S.; Yang, G.; Yang, Z.; Liu, P.-J.; Yan, Q.-L. Energetic metastable n-Al@PVDF/EMOF composite nanofibers with improved combustion performances. *Chem. Eng. J.* **2020**, *383*, 123146. [CrossRef]
4. Ma, X.; Li, Y.; Hussain, I.; Shen, R.; Yang, G.; Zhang, K. Core–shell structured nanoenergetic materials: Preparation and fundamental properties. *Adv. Mater.* **2020**, *32*, e2001291. [CrossRef]
5. Tang, D.; Chen, S.; Liu, X.; He, W.; Yang, G.; Liu, P.-J.; Gozin, M.; Yan, Q.-L. Controlled reactivity of metastable n-Al@Bi(IO3)3 by employment of tea polyphenols as an interfacial layer. *Chem. Eng. J.* **2020**, *381*, 122747. [CrossRef]
6. Zhu, Y.; Zhou, X.; Wu, C.; Cheng, H.; Lu, Z.; Zhang, K. Si wire supported MnO2/Al/fluorocarbon 3D core/shell nanoenergetic arrays with long-term storage stability. *Sci. Rep.* **2017**, *7*, 6678. [CrossRef]
7. Weismiller, M.R.; Huba, Z.J.; Epshteyn, A.; Fisher, B.T. Combustion of sonochemically-generated Ti−Al−B nanopowders in a premixed methane/air dust flame. *Combust. Flame* **2018**, *191*, 187–194. [CrossRef]
8. Lee, H.; Deshmukh, P.; Kim, J.H.; Hyun, H.S.; Sohn, Y.; Shin, W.G. Spray drying formation of metal oxide (TiO2 or SnO2) nanoparticle coated boron particles in the form of microspheres and their physicochemical properties. *J. Alloys Compd.* **2019**, *810*, 151923. [CrossRef]
9. Yuan, G.; Su, S. Preparation and characterization of poly (styrene-Co-maleic anhydride)-modified boron particles. *J. Dispers. Sci. Technol.* **2010**, *31*, 327–331. [CrossRef]
10. Cheng, L.; Yang, H.; Yang, Y.; Li, Y.; Meng, Y.; Li, Y.; Song, D.; Chen, H.; Artiaga, R. Preparation of B/Nitrocellulose/Fe particles and their effect on the performance of an ammonium perchlorate propellant. *Combust. Flame* **2020**, *211*, 456–464. [CrossRef]

11. Young, G.; Stoltz, C.A.; Mayo, D.H.; Roberts, C.W.; Milby, C.L. Combustion behavior of solid fuels based on PTFE/boron mixtures. *Combust. Sci. Technol.* **2013**, *185*, 1261–1280. [CrossRef]
12. Matsumoto, K.; Itoh, Y.; Kameda, T. EB-PVD process and thermal properties of hafnia-based thermal barrier coating. *Sci. Technol. Adv. Mater.* **2003**, *4*, 153–158. [CrossRef]
13. Glotov, O.; Poryazov, V.; Surodin, G.; Sorokin, I.; Krainov, D. Combustion features of boron-based composite solid propellants. *Acta Astronaut.* **2023**, *204*, 11–24. [CrossRef]
14. Keerthi, V.; Nie, H.; Pisharath, S.; Hng, H.H. Combustion Characteristics of Fluoropolymer Coated Boron Powders. *Combust. Sci. Technol.* **2020**, *194*, 1183–1198. [CrossRef]
15. He, W.; Liu, P.; He, G.; Gozin, M.; Yan, Q. Highly Reactive Metastable Intermixed Composites (MICs): Preparation and Characterization. *Adv. Mater.* **2018**, *30*, e1706293. [CrossRef]
16. Xie, Z.Y.; Zhou, L.; Wang, H.; Zhao, K.; Luo, Y.M.; Zhang, H.L. Combustion Performance of Boron Coated with AP. *Acta Armamentarii* **2014**, *35*, 194–199. [CrossRef]
17. Cheng, L.; Yang, H.; Majeed, M.A.; Li, Y.; Song, D.; Li, Y. B/Metal composites' thermochemical properties and their effect on the performance of an ammonium perchlorate propellant. *J. Energetic Mater.* **2021**, *39*, 344–360. [CrossRef]
18. Liu, R.; Yang, D.F.; Zhang, Y.L.; Nie, H.Q.; Yan, Q.L. Preparation and Properties of Halogenated Oxidant Coated Modified Boron with High Combustion Efficiency. *Chin. J. Energetic Mater.* **2024**, *32*, 1068–1079. [CrossRef]
19. Ke, X.; Guo, S.; Zhang, G.; Zhou, X.; Xiao, L.; Hao, G.; Wang, N.; Jiang, W. Safe preparation, energetic performance and reaction mechanism of corrosion-resistant Al/PVDF nanocomposite films. *J. Mater. Chem. A* **2018**, *6*, 17713–17723. [CrossRef]
20. Mao, H.; Zhang, X.; Cui, R.; Zhang, C.; Zhou, X. Preparation of Si@PVDF composite microspheres by electrostatic spraying for enhanced energetic characteristics. *Combust. Flame* **2023**, *252*, 112740. [CrossRef]
21. Liu, J.; Wang, D.; Zhang, Z.; Li, F. Improvement of the Ignition Performance and Reaction Rate of Boron by Surface Modification. *Combust. Explos. Shock Waves* **2024**, *60*, 110–118. [CrossRef]
22. Chintersingh, K.-L.; Sun, Y.; Schoenitz, M.; Dreizin, E.L. Heterogeneous reaction kinetics for oxidation and combustion of boron. *Thermochim. Acta* **2019**, *682*, 178415. [CrossRef]
23. Hu, X.L.; He, H.J.; Wang, L.Y.; Yang, C.H.; Yao, X.X.; Zhou, W.L.; Xiao, L.Q.; Liu, S.E.; Liu, J.F. The effect of compounding methods of binder on the thermal properties of boron powder. *J. Ordnance Equip. Eng.* **2024**, *45*, 223–229. [CrossRef]
24. Liu, C.; Fan, H.J.; Li, Z.Y.; Guan, C.H.; Li, H.; Qi, X.F. Combustion Characteristics of CMDB Propellant Containing Ball-boron Powder. *Initiat. Pyrotech.* **2017**, *3*, 38–40. [CrossRef]
25. Lebedeva, E.A.; Astaf, S.A.; Istomina, T.S.; Badica, P. Combustion products agglomeration of propellant containing boron with fluorinated coatings. *Combust. Flame* **2022**, *238*, 111749. [CrossRef]
26. Chaturvedi, S.; Dave, P.N. Solid Propellants: AP/HTPB Composite Propellants. *Arab. J. Chem.* **2019**, *12*, 2061–2068. [CrossRef]
27. Wang, F.; Jiang, X.B.; Ma, L.; Ba, S.H.; Wang, X.F.; Mei, Q.H. Study on Interface Modification of Boron Powder and Its Properties in Ignition Powder. *Initiat. Pyrotech.* **2022**, *2*, 39–42. [CrossRef]
28. Xu, H.X.; Zhao, F.Q. Characteristics of high purity boron powder and its application in boron-based fuel-rich propellant. *J. Solid. Rocket. Technol.* **2008**, *31*, 368–373. [CrossRef]
29. Ulas, A.; Kuo, K.K.; Gotzmer, C. Ignition and combustion of boron particles in fluorine-containing environments. *Combust. Flame* **2001**, *127*, 1935–1957. [CrossRef]


**Disclaimer/Publisher's Note:** The statements, opinions and data contained in all publications are solely those of the individual author(s) and contributor(s) and not of MDPI and/or the editor(s). MDPI and/or the editor(s) disclaim responsibility for any injury to people or property resulting from any ideas, methods, instructions or products referred to in the content.